

A reversible decoration of multi-walled carbon nanotubes (MWCNTs) by acyclic η^4 -(1*E*,3*E*)-dienyl-Fe(CO)₃ complexes†

Jean-Paul Lellouche,^{*a} Maytal Piran,^a Lior Shahar,^a Judith Grinblat^a and Christophe Pirlot^b

Received 15th October 2007, Accepted 9th January 2008

First published as an Advance Article on the web 1st February 2008

DOI: 10.1039/b715913g

Selected acyclic disubstituted η^4 -(1*E*,3*E*)-dienyl-Fe(CO)₃ iron complexes presented a non-covalent, but reversible affinity for multi-walled carbon nanotube (MWCNT) sidewalls likely mediated by hydrophobic and/or π - π stacking interactions. Resulting iron-complexed MWCNT-based composites displayed methyl ester/acetate, aldehyde and/or OH functional groups on CNT sidewalls. They displayed strong FT-IR absorption peaks due to organometallic C \equiv O groups of the Fe(CO)₃ unit ($\nu_{\text{C}\equiv\text{O}} = 1966\text{--}2068\text{ cm}^{-1}$). These peaks appeared in an absorption window free of any parasitic band that usually characterize organic/bio-organic species. Routine FT-IR spectroscopy enabled an effective tracking of adsorption processes of iron complexes onto MWCNT sidewalls. Iron-complexed MWCNTs may be readily dissociated using CH₃CN, allowing an accurate weight quantification of adsorptions. Both interacting components remained unmodified after composite dissociation. Sidewall oxygenated defects at high concentration were also shown to be detrimental to iron complex adsorption. This quantitative decoration methodology may constitute a quite unusual application in the Quality-Control (QC)-driven standardization/improvement of the industrial production of MWCNTs (detection of MWCNT sidewall oxygenated defects during fabrication and purification).

1. Introduction

Carbon nanotubes (CNTs) are new fullerene-related carbon-based nanostructures, which consist of one or several graphene sheets of sp²-hybridized carbon hexagons disposed coaxially around an internal hollow cavity.^{1–4} CNTs possess a quite unique set of mechanical, electrical, and magnetic properties making them particularly attractive for various (bio)nanotechnology applications. Moreover, they may be readily functionalized when targeting CNT pentagon-containing end-caps sensitive to oxidation and/or the outer 1D extended π -conjugated system (CNT sidewall). For example, CNT oxidation generated end/sidewall-localized COOH groups that were exploited for the covalent attachment of (bio)molecular probes,^{5–8} polymers,⁹ and metallic particles.¹⁰ Other covalent modifications of CNT

π -conjugated sidewalls include 1,3-dipolar cycloadditions of azomethine ylides,¹¹ electrophilic fluorinations,^{12,13} and electrophilic additions of aryl diazonium salts.¹⁴

Unlike covalent modifications, non-covalent functionalizations are based on van der Waals and/or π - π stacking interactions.^{5–8,15–21} They did not alter the carbon sp²-hybridized curved CNT sidewall structure of corresponding CNT-containing nanocomposites. For that purpose, CNT sidewalls were non-covalently decorated with a range of hydrophobic and unsaturated compounds,^{15–17} polymers [polyethyleneimine, poly(aryleneethynylene)s, poly(methyl methacrylate), poly(ethylene glycol)],^{18–19} surfactants (triton, sodium dodecyl sulfate),²⁰ pyrene-containing species (*N*-succinimidyl-1-pyrenebutanoate),²¹ peptidic amphiphiles,²² and proteins presenting hydrophobic and/or π -unsaturated domains (bovine serum albumin, streptavidin, Zn–Cd metallothionein).²¹

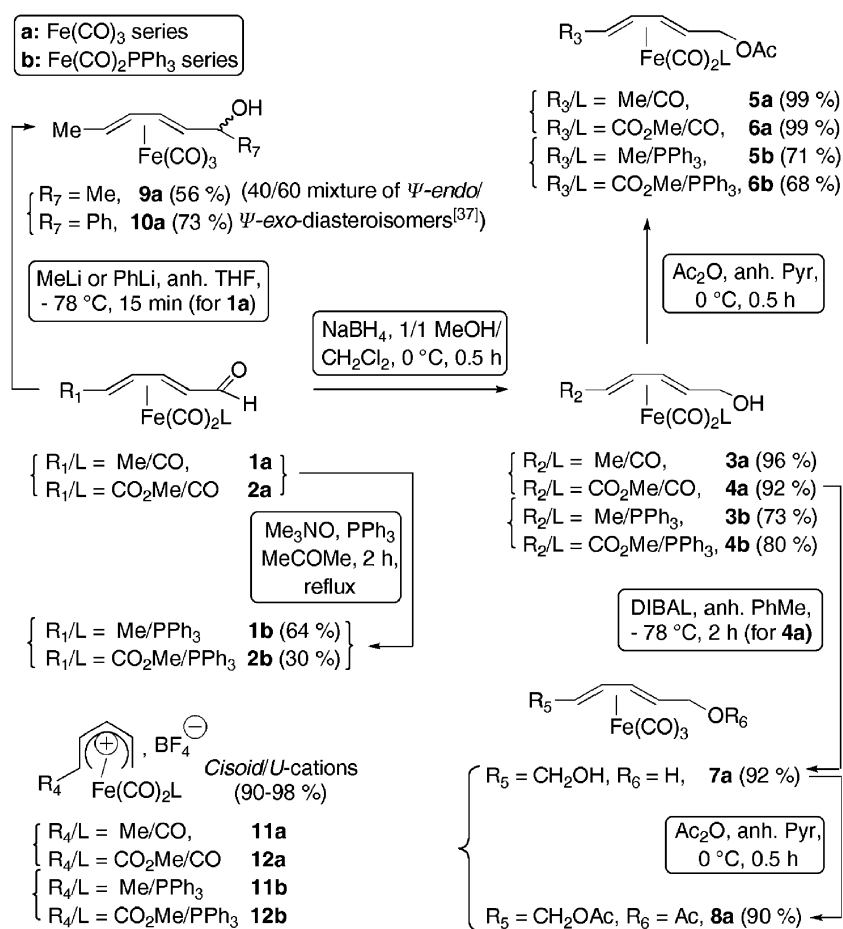
To what extent such dual-component association processes may be *totally* or *partially reversible* remains an intriguing open question in the field. More specifically, no process has ever been described and characterized as *fully reversible and controlled* regarding association/dissociation conditions. An immediate consequence of process reversibility would be its quantification. In cases where both components would not have undergone any structure modification, component recycling would be an additional strong asset. Such improved features will certainly impact various CNT-based applications, such as the establishment of improved standards of Quality-Control (QC) for the industrial production of CNTs and the development of recyclable electronic (bio)sensors based on CNTs/CNT arrays.

Here, we demonstrate that selected acyclic disubstituted η^4 -(1*E*,3*E*)-dienyl-Fe(CO)₃ iron complexes^{23–25} (Scheme 1) show a *non-destructive and reversible affinity* for sidewalls of MWCNTs.

^aDepartment of Chemistry, Institute of Nanotechnology and Advanced Materials, Faculty of Exact Sciences, Bar-Ilan University, 52900 Ramat-Gan, Israel. E-mail: lellouj@mail.biu.ac.il

^bNanocyl s.a., 4 Rue de l'Essor, B-500 Sambreville, Belgium

† Electronic supplementary information (ESI) available: Illustrative photographs of the experimental process of complex adsorptions, FT-IR spectra of iron-complexed composites [MWCNT-Fe(CO)₃], a table of characteristic metallic Fe-C \equiv O FT-IR absorption peaks, high resolution SEM and TEM pictures of MWCNTs decorated by iron complex **5a** (including EDAX/EDS linescan elemental analyses), selected XPS data for MWCNTs decorated by neutral iron complexes **1a**, **3a–4a**, and **7a–8a**, XPS data for untreated and oxidized MER MWCNTs, high resolution SEM pictures and EDAX analyses of MWCNTs obtained *after* iron complex desorption (case of the CH₃CN-dissociated composite MWCNT-**5a**), Global-Energy GMMX-minimized structures of *effective* and selected *ineffective* complexes, **1a**, **3a–4a**, **6a–8a**, and ψ -*endo*/ ψ -*exo*-**9a** and **10a**, an illustrative TGA graph of composite MWCNT-**5a**, and Raman spectra of untreated starting MWCNTs and of MWCNTs obtained *after* CH₃CN-mediated dissociation of composite MWCNT-**5a**. See DOI: 10.1039/b715913g



Scheme 1 Acyclic η^4 -(1E,3E)-dienyl and η^5 -pentadienyl-Fe(CO)₂L iron complexes (L = CO or PPh₃).

The decoration process resulted in new MWCNT-based nanomaterials, iron-complexed MWCNTs [MWCNT-Fe(CO)₃], which can be dissociated using specific washing conditions. Since interacting complexes are functional, resulting [MWCNT-Fe(CO)₃] composites displayed the same chemical functions, methyl ester/acetate, aldehyde, OH, which may be useful for post-adsorption functionalization. Additionally, strong FT-IR absorptions of organometallic carbonyl groups of the Fe(CO)₃ unit ($\nu\text{C}\equiv\text{O} = 1966\text{--}2068 \text{ cm}^{-1}$)^{26,27} appeared in an absorption window free of the parasitic bands commonly observed for biological and non-biological species. This specific spectroscopic feature enabled quite effective FT-IR traceability of complex adsorptions/desorptions during component association/dissociation. We also disclosed preliminary data, which indicate an opposite relationship between adsorption effectiveness of iron complexes and increased concentrations of oxygenated defects present on MWCNT sidewalls. These last results emphasized the interesting potential of this innovative MWCNT functionalization methodology for the delivery of high-quality industrially processed MWCNTs (traceability of MWCNT defects towards Quality-Control standardization).

2. Experimental

2.1. Instrumentation

FT-IR spectroscopy. IR spectral data were collected using a Nicolet IMPACT 410 Instrument. KBr pellets were consistently

prepared by diluting 0.2 mg of an iron-complexed MWCNT-Fe(CO)₃ composite with 200.0 mg of dry IR grade KBr (Aldrich). Under these conditions, IR transmissions were always maintained better than 85%. Higher concentrations of MWCNT-based composites caused sample opacity.

High resolution (HR) transmission and scanning electron microscopies (HR-TEM/HR-SEM) and elemental energy-dispersive X-ray spectroscopy

HR-TEM. Microphotographs were obtained from a JEOL JEM-2010 instrument (Oxford Instruments, accelerating voltage 200 kV, Gatan CCD camera). Carbon-free 400 mesh Au grids (Agar Scientific Ltd., UK) have been used for sample preparation. Compositional characterizations of samples (elemental EDAX analyses) used Inca software (Oxford Instruments). Dry samples (1.0 mg) have been suspended in EtOH (1.0 mL) under sonication (Cole Parmer 8891 ultrasonic bath, 5 min, 20 °C) before deposition/solvent evaporation on a carbon-free Au grid.

HR-SEM. Microphotographs were obtained from a JEOL JSM-7000 P apparatus (Oxford Instruments, accelerating voltage, Gatan CCD camera). Samples (1.0 mg) were deposited on a small carbon tape surface (1 cm²) fixed on a well-cleaned Cu grid, followed by optional gold evaporation under vacuum, when indicated.

Compositional characterizations of samples, elemental EDAX/EDS Linescan and STEM mapping/EDAX spectrometer map analyses used an Inca software (Oxford Instruments).

X-Ray photoelectron spectroscopy (XPS). XPS analyses were carried out using a Kratos Axis HS apparatus equipped with an ultra-high vacuum chamber (5×10^{-10} torr) containing samples loaded onto a double-sided carbon-based self-adhesive tape (complete coverage). Survey spectra were acquired at a PE (pass energy) of 80 eV and 0.5 eV incremental steps, with a standard monochromatized Al K α source at 75 W. Sample measurements were performed under a low-energy electron flood (gun operation) for charge neutralization. Resulting photoemission spectra were analyzed with a "Vision 2" package from Kratos. Binding energy data were compared to those appearing in the NIST database (<http://srdata.nist.gov/xps>) after spectrum calibration *vs.* the C 1s peak at 285 eV.

Thermogravimetric analysis (TGA). TGA graphs were run on a Thermofinnigan TA Q600-0348 (model SDT Q600) apparatus with a temperature profile setting being 50–800 °C at 20 °C min⁻¹ under N₂.

Raman spectroscopy. Raman measurements were collected using a Jobin Yvon Micro Raman instrument (Model HR800, excitation wavelength: $\lambda = 632.8$ nm, laser power: 15 mW, slit size = 100 μ m, hole = 1000 μ m). Corresponding spectra were obtained by accumulation of two 2 s long scans (X100 objective lens for a 1.0 μ m spot size).

2.2. Synthesis

Preparation of acyclic cationic and non-cationic iron complexes in both CO and PPh₃ series. Neutral η^4 -(1*E*,3*E*)-dienyl- and cationic U-shaped isolated η^5 -pentadienyl-Fe(CO)₂L (L = CO or PPh₃, **a** or **b** series, Scheme 1) iron complexes tested in this study have been readily prepared using well-known procedures: Fe₂CO₉-mediated complexations of (1*E*,3*E*)-dienes,^{23–25} Me₃NO-mediated C \equiv O to PPh₃ ligand exchanges,²⁸ complex-stereodirected

nucleophilic additions of organolithium reagents onto adjacent carbonyl functions,^{23–25} and complex-assisted Lewis acid-mediated ionizations.^{23–25,29} More specifically, all the related detailed synthetic procedures and characterization data of neutral and cationic iron complexes tested in adsorption experiments onto MWCNT sidewalls have been gathered in ref. 30. Corresponding reaction yields have been also reported and were unoptimized.

2.3. Non-covalent adsorption experiments of iron complexes in aqueous and non-aqueous media

Adsorption experiments with iron-complexed species (Scheme 1) used MWCNTs of high-purity produced by catalytic CVD [MER Corporation, averaged diameter/length: 35 (\pm 10) nm/30 μ m, 78–140 graphitic layers, purity \approx 98.0 % by TGA analysis, less than 2.0 and 0.1% of amorphous graphitic contaminants and iron (Fe catalyst) respectively, 50.0 or 200.0 mg depending on adsorption protocols].

Two sets of experimental conditions were set up depending on the *neutral* or *cationic* water-sensitive type of complexes involved. They related to the DMF- or CH₂Cl₂ (DCM)-based *aqueous* and *non-aqueous* protocols detailed below.

A typical DMF-based aqueous protocol for iron complex adsorption. Neutral water-compatible η^4 -(1*E*,3*E*)-dienyl-Fe(CO)₂L (L = CO and/or PPh₃) iron complexes **1–10** (**a** and/or **b** series respectively, 0.110–0.180 mmol) were tested using a DMF-based aqueous protocol [photographs 1A–1C, ESI†, p. 2]. As disclosed later in this study (Table of adsorption data, Table 1), this method maximized hydrophobic and/or van der Waals interactions of iron complexes with hydrophobic MWCNT sidewalls. Accordingly, a minimal volume of water-compatible DMF in regard to the total reaction volume (0.25 *versus* 5.25 mL respectively) has been used for complex solubilization before addition into water-suspended MWCNTs (50.0 mg, 5.0 mL of distilled H₂O). Complex addition caused the immediate formation of a milky precipitation/suspension of the complex (photograph 1B, ESI†, p. 2), which vanished progressively. One obtained two distinct phases, a yellowish

Table 1 Non-covalent adsorption of selected neutral iron complexes onto MWCNTs: quantitative weight data (from CH₃CN washing experiments and TGA analyses)

Entry	Complex	Adsorbed complex			
		DCM-protocol CH ₃ CN/mg (μ mol) ^{a,c}	DMF-protocol CH ₃ CN/mg (μ mol) ^{b,c}	Calculated data (%) ^{b,d}	TGA data (%) ^{b,e}
1	1a	4.20 (14.7)	7.99 (28.0)	13.78	10.44
2	3a	10.48 (20.1)	10.24 (20.0)	17.00	14.85
3	4a	13.50 (47.0)	16.62 (58.0)	24.95	22.38
4	5a	9.10 (31.0)	20.40 (73.0)	28.98	28.13
5	6a	8.60 (25.0)	19.00 (67.0)	27.54	24.04
6	7a	5.70 (22.0)	13.22 (52.0)	20.91	18.22
7	8a	4.43 (13.0)	1.10 (4.0)	1.86	— ^f

^a Non-aqueous DCM-based adsorption protocol—use of 200.0 mg of MWCNTs. ^b DMF-based aqueous adsorption protocol—use of 50.0 mg of MWCNTs. ^c Weight data obtained after composite dissociation: CH₃CN washing (triplicate experiments for each entry). ^d Calculated weight data (in weight loss percent) for the case of the CH₃CN-mediated dissociation of [MWCNT-Fe(CO)₃] nanocomposites prepared using the DMF-based aqueous protocol. ^e Weight data determined by TGA analysis performed on [MWCNT-Fe(CO)₃] nanocomposites prepared using the DMF-based aqueous protocol (for the weight loss percentage, the temperature range for complex decomposition/burning: 117–252 °C). ^f No observable weight decrease (background signal) due to the limited sensitivity of TGA measurement.

homogeneous aqueous phase, which contained the tested complex in excess, and decanted iron-complexed MWCNTs, *i.e.* [MWCNTs-Fe(CO)₃] (photograph 1C, ESI†, p. 2). Following adsorption completion (2 h, room temperature), the resulting iron-complexed MWCNTs were washed several times by neutral H₂O (5 × 5.0 mL H₂O, centrifugation steps operated at 7500 rpm for 15 min, 20 °C) until a colorless aqueous phase was obtained (elimination of iron complexes in excess). A simple TLC checking/follow-up of successive washing aqueous phases (silica gel Merck 60F₂₅₄ thin chromatography plates, 1/1 v/v hexane/ethyl acetate solvent mixture) confirmed this visual test. The cleaned iron-complexed MWCNTs were then dried under high vacuum (1 × 10⁻⁶ mm Hg, 2 h, 20 °C) before further manipulation (dissociation experiments using CH₃CN for adsorption quantification, Table of adsorption data, Table 1) and/or composite characterization.

A typical non-aqueous DCM-based protocol for iron complex adsorption. MWCNTs (200.0 mg) were gently shaken with neutral and/or water-sensitive cationic iron complexes **1–12** (L = CO or PPh₃, **a** and/or **b** series respectively, 0.110–0.180 mmol) in anhydrous DCM (5.25 mL) at room temperature for 2 h. Following adsorption completion, iron-complexed MWCNTs were decanted by centrifugation (7500 rpm for 15 min, 20 °C, homogeneous yellow dichloromethane phase), and washed (5 × 5.0 mL DCM, then centrifugation: 7500 rpm for 15 min, 20 °C) until a colorless organic phase was obtained (TLC checking for complex presence, see details above). They were dried under vacuum (1 × 10⁻⁶ mm Hg, 2 h, 20 °C) and stored before characterization and/or dissociation experiments (adsorption quantification). Since they are less effective, CH₂Cl₂-mediated complex adsorptions were always performed on a *four times greater quantity* of MWCNTs (200.0 mg) in order to get precise weight measurements of adsorbed/dissociated complexes (Table of adsorption data, Table 1).

Results and discussion

Adsorption experiments and characterization of iron-complexed multi-walled carbon nanotubes [MWCNTs-Fe(CO)₃]

Among all the neutral complexed species tested using the aqueous protocol, *the seven neutral iron complexes, 1a and 3a–8a* (Scheme 1),³⁰ showed a measurable affinity toward MWCNT sidewalls in the 4.0–73.0 μmol (1.10–20.40 mg) range (*triplicate experiments*, Table of adsorption data, Table 1, entries 1–7).

Preliminary FT-IR analyses were performed on dried decorated MWCNTs. They confirmed the presence of two strong νFe–C≡O absorptions that are characteristic of irontricarbonyl species,^{26–27} (KBr pellet, νFe–C≡O = 1966–1994 and 2047–2068 cm⁻¹, FT-IR data/spectra: Fig. 1 and ESI†, p. 3–7). In addition, the typical iron-complexed composite MWCNT-**5a** was thoroughly characterized by HR-SEM and HR-TEM. Fig. 2A and C depict HR-SEM microphotographs of bundles of complex-modified MWCNTs of various diameters (130 nm–1.0 μm).³¹ The observed surface roughness was likely due to complex adsorption, as confirmed by EDAX elemental analysis [Fig. 2B and D, the presence of iron-rich surfaces, see ESI (p. 8–10) for additional microphotographs and EDAX elemental/EDS linescan analyses].

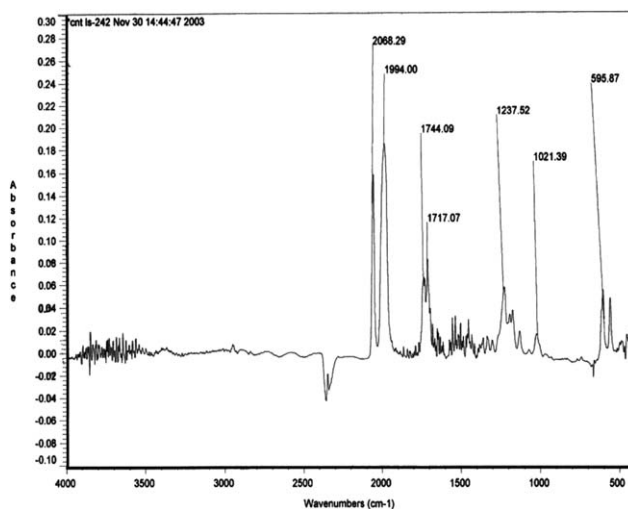


Fig. 1 FT-IR spectrum of cleaned MWCNTs decorated by iron complex **6a** and showing the presence of two intense absorption peaks of organometallic Fe–C≡O groups at 1994.0 and 2068.3 cm⁻¹.

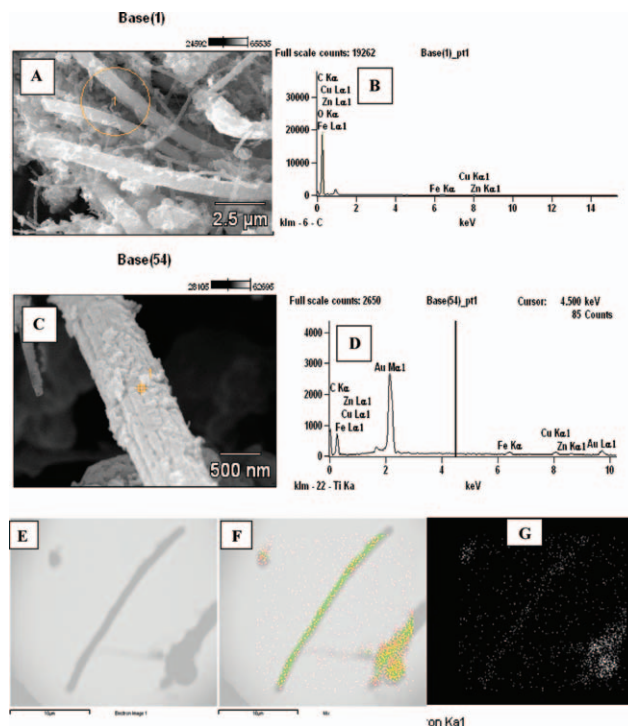


Fig. 2 A and C: HR-SEM images of MWCNTs decorated by **5a** (magnifications: 10 000× and 35 000×) and related EDAX analyses (B and D) showing an iron-rich surface (C and D: Au-evaporated sample). F and G: STEM analysis/EDAX spectrometer maps showing the distribution of iron (Fe, red & white colors) and carbon (C, green color) elements (microphotographs F & G).³² Same unmaped objects were visualized in microphotograph E.

HR-TEM microscopy combined with EDAX elemental analyses also showed MWCNT surface-localized black iron-rich islets arising from the destruction of **5a** caused by the high-energy electron irradiation (see corresponding HR-TEM microphotographs and EDAX data in the ESI†, p. 11).

Moreover, an elemental map of a 30 μm long bundle of the same iron-complexed composite MWCNT-**5a** (STEM mapping analysis using Inca software, data acquisition time: 24.0 h, Fig. 2F and G) confirmed the distribution homogeneities of both iron (*red & white* colors) and carbon (*green* color) elements on its surface.³²

For the sake of comparison, the same unmapped objects were also visualized in Fig. 2E. Additional proof of the successful surface modification of MWCNTs by iron complexes **1a**, **3a–4a**, and **7a–8a** arose from XPS spectroscopy (ESI†, p. 12–16). It showed the presence of narrow Fe 2p 3/2 peaks at 709.0 eV, characteristic of iron species in a low oxidation state [Fe(0) oxidation state of adsorbed complexes], and in interaction with C \equiv O ligands (comparison with binding energies registered in the NIST database: <http://srdata.nist.gov/xps>).

Iron-complexed composites [MWCNT-Fe(CO)₃] were stable when suspended for 2 h in several organic/aqueous solvents [DMF, cold CH₂Cl₂, CH₃COCH₃, MeOH, THF, hot H₂O (80 °C), neutral 0.01 M PBS buffer; FT-IR/TLC monitoring of iron complex desorption]. On the other hand, a unique CH₃CN washing (3 \times 10.0 mL) of composites enabled the complete desorption of iron complexes and their quantification for both adsorption protocols (Table of adsorption data, Table 1, triplicate experiments, entries 1–7). The data consistency for complex adsorption was checked as follows: weight measurements obtained for composites prepared using the most effective aqueous DMF-based protocol could be readily calculated as weight loss percentages (Table of adsorption data, Table 1). Resulting percentage data were compared with similar weight loss measurements obtained by another method, *i.e.* thermogravimetric analysis (Table of adsorption data, Table 1). All tested composites disclosed iron complex decomposition and/or burning as a one-step weight loss arising between 117–252 °C (see the illustrative TGA curve of composite MWCNT-**5a**, ESI†, p. 24). The composite MWCNT-**8a** (entry 7) could not afford any measurable weight loss, most likely due to a lack of sensitivity of the TGA method. Interestingly, weight loss data obtained by TGA followed the same order of decoration effectiveness as the one disclosed in CH₃CN-mediated dissociation experiments. CH₃CN-based weight data were also found to be higher than weight losses measured by TGA. This may be explained by a putative heat-dependent chemical modification of MWCNT sidewalls during complex decomposition/burning [transfer/attachment of the Fe(CO)₃ unit onto graphene-localized (1,3)/(1,4)-dienes followed by decomposition].^{33,34}

Importantly, all the retrieved CH₃CN-dissociated iron complexes remained structurally unmodified according to TLC (co-spotting with reference compounds), FT-IR, and high-resolution ¹H/¹³C-NMR analyses. On the other hand, and relating to the insoluble MWCNT component, two selected CH₃CN-dissociated MWCNT samples obtained from iron-complexed composites, MWCNT-**5a** and MWCNT-**6a**, as well as untreated MWCNTs as a reference, were analyzed in parallel by HR-SEM, including EDAX elemental analysis. The iron (Fe) element could not be detected in these samples (see illustrative HR-SEM microphotographs and EDAX analyses relating to the CH₃CN-dissociated MWCNT sample arising from composite MWCNT-**5a**, ESI†, p. 17–18). Raman spectroscopy of the same MWCNT samples exhibited the expected typical structure

of MWCNTs, presenting both defect- and graphite-mode D and G bands of similar shapes at 1351.5 and 1583.1 cm⁻¹, respectively^{35,36} (ESI†, p. 25).

Moreover, *two additional cycles of adsorption–dissociation* for all effective complexes were successfully repeated without any observed erosion of complex adsorption capabilities. Thus, sequential iron complex adsorptions and CH₃CN-mediated desorptions did not affect the graphene structure of MWCNT sidewalls. All these combined results emphasized the full reversibility of iron complex adsorptions onto MWCNTs that were most likely mediated by *non-covalent* van der Waals and/or π – π stacking interactions.

Quantitatively speaking, the following increasing order in adsorption efficiency for effective complexes has been found (Table of adsorption data, Table 1): **8a** (4.0 $\mu\text{mol}/1.10$ mg) < **3a** (20.1 $\mu\text{mol}/10.24$ mg) \sim **1a** (28.0 $\mu\text{mol}/7.99$ mg) < **7a** (52.0 $\mu\text{mol}/13.22$ mg) \approx **4a** (58.0 $\mu\text{mol}/16.62$ mg) < **6a** (67.0 $\mu\text{mol}/19.00$ mg) < **5a** (73.0 $\mu\text{mol}/20.40$ mg). This order did not reflect the expected water solubilities of corresponding complexes. For example, monoalcohol **3a** was less efficiently adsorbed than the more hydrophobic acetate **5a** (entries 2 and 4). A similar trend was also observed for the ester alcohol **4a** and the more hydrophobic ester acetate **6a** (entries 3 and 5). DCM-mediated adsorptions performed on a *four-fold* greater quantity of MWCNTs (200.0 mg) confirmed the effectiveness of the same complexes, but at a lower efficiency range (13.0–47.0 $\mu\text{mol}/4.43$ –13.50 mg). In that case, a slightly modified order of efficiency was obtained: **8a** \approx **1a** < **3a** \approx **7a** < **6a** < **5a** < **4a**, but the same triad, **4a–6a**, of more effective complexes remained unchanged for both protocols (Table of adsorption data, Table 1, entries 3–5). In contrast, cationic charge-deficient U-shaped iron complexes **11a/b–12a/b** [Fe(i) oxidation state], and consequently, equilibrated isomeric S-shaped ones,^{23–25} presented no affinity for MWCNT sidewalls. Both protocols also had in common the fact that neither neutral PPh₃-substituted nor α -substituted iron complexes **1b–6b** and **9a–10a** (40/60 mixture of ψ -*endo*/ ψ -*exo* diastereoisomers³⁷) were successfully adsorbed.

A tentative adsorption model has been elaborated in order to rationalize these results (Fig. 3a). It relied on the well-known *anti* stereodirecting properties of the Fe(CO)₂L organometallic unit (L = CO or PPh₃).^{23–25} Accordingly, adsorption of effective complexes onto MWCNT sidewalls most likely occurred *via* the complex planar C α –C ϵ dienyl side in an *anti* manner from the Fe(CO)₂L unit. Therefore, developing van der Waals and/or π – π stacking interactions may be maximized during complex adsorption. Additionally, α -located R/R₈ substituents must be of minimal steric requirement in order to be positioned *syn* to the organometallic unit. This spatial disposition should enable the simultaneous minimization of both types of nonbonding interactions indicated in Fig. 3a, intramolecular side and R/R₈-based interactions involving the MWCNT graphene surface. Both demands must be satisfied simultaneously for an effective complex adsorption. Accordingly, structure minimizations of selected η^4 -(1*E*,3*E*)-dienyl-Fe(CO)₃ iron complexes were calculated with the energy minimization program for global-energy minima GLOBAL-MMX (GMMX) during random conformational searching (PCMODEL V8.0 software, Serena Software, Bloomington, USA). Its Allinger MM2-derived MMX force field enabled the handling of such

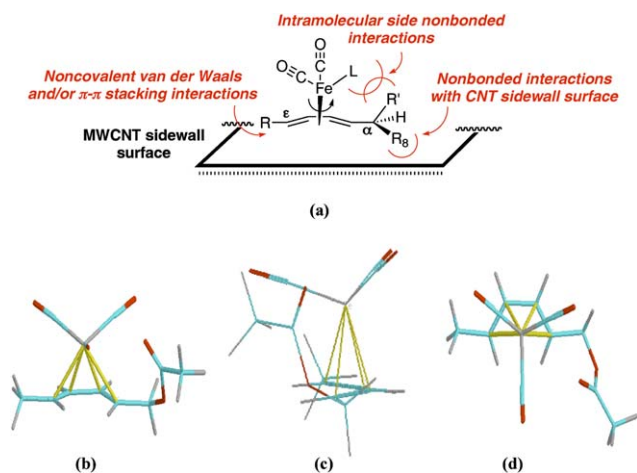


Fig. 3 (a) Model of nonbonding interactions that developed during complex adsorption onto the MWCNT sidewall (illustrated for $L = \text{CO}$ or PPh_3 and $R/R_8 = \text{H, OH}$, or any other indicated substituent—see text), and (b–d) global-energy GMMX-minimized structures of iron complex **5a** (front, side and top views, respectively, $\text{C}\beta\text{C}\gamma\text{-C}\delta\text{C}\epsilon$ dihedral angle = 7°)

$\eta^4\text{-}(1E,3E)\text{-dienyl-Fe}(\text{CO})_3$ iron complexes. Conformational space searching included all rotatable bonds of a given structure using default bond rotation increment settings and stop criteria defined by the software. GMMX-minimized structures of all effective irontricarbonyl complexes, **1a**, **3a–8a**, and selected ineffective ones, $\psi\text{-endo}/\psi\text{-exo-9a}$ and **10a**, were obtained (Figs. 3b–d, and ESI†, p. 19–22). This allowed some interesting observations to be drawn:

First, polar R/R_8 substituents, which included aldehyde/ester $\text{C}=\text{O}$, primary CH_2OH /secondary CHOH , and CH_2OAc groups, were always spatially located *syn* to the $\text{Fe}(\text{CO})_3$ organometallic unit, most likely because of favorable polar interactions with organometallic $\text{C}\equiv\text{O}$ groups. This is particularly clear for both α -phenyl/methyl substituted diastereoisomeric iron-complexed alcohols $\psi\text{-endo}/\psi\text{-exo-9a}$ and **10a** (ESI†, p. 21–22), although they were found to be ineffective. In that case, GMMX-minimized structures emphasized detrimental nonbonding interactions between α -located phenyl/methyl groups and the MWCNT graphene surface, resulting in non-adsorption. Second, calculated values for all complex dihedral angles, $\text{C}\beta\text{C}\gamma\text{-C}\delta\text{C}\epsilon$, varied in a small $0\text{--}7^\circ$ range (ESI†, p. 22). Thus, a minimal distortion from the planarity of the complex dienyl-face did not preclude effective $\pi\text{-}\pi$ interactions with the MWCNT sidewall graphene surface. Similar structural trends also appeared for GMMX-minimized structures of two illustrative, but ineffective PPh_3 -substituted iron complexes **5b** and **6b** (minimized structures not shown). The stronger hydrophobicity of PPh_3 - versus $\text{Fe}(\text{CO})_3$ -substituted iron complexes likely explained this discrepancy in adsorption behavior. Indeed, these complexes were insoluble in the DMF-containing aqueous medium (TLC checking). On the other hand, and for PPh_3 -substituted iron complexes, non-aqueous DCM-based conditions caused the solvent itself to successfully compete with the MWCNT surface. It resulted in complex nonadsorption (competition between complex bulk dissolution and complex adsorption onto the MWCNT surface, respectively).

On further investigation, effective iron complexes, **1a**, and **3a–8a**, were examined for their ability to sense sidewall-localized oxygenated defects ($\text{C}=\text{O}$, $\text{C}-\text{OH}$, and COOH) in end-opened oxidized MWCNTs. Known mild acidic and oxidizing conditions (1 : 1 mixture of $\text{HNO}_3\text{-H}_2\text{SO}_4$, 70°C , 2 h) have been employed for this purpose.^{38,39} Compositional values in carbon (C, C 1s) and O (oxygen, O 1s) were determined by XPS for both *untreated* and *oxidized* MER Corporation MWCNTs (C: 93.4 and 68.9 %, O: 6.0 and 27.2 % for untreated and treated MWCNTs respectively, ESI†, p. 23). As a result, none of the effective iron complexes were successfully adsorbed using either the DMF- or DCM-based protocol. These data emphasized a clear opposite relationship between the efficiency of iron complex adsorptions and the structural integrity of the MWCNT graphene sidewall (defect presence). Interestingly, MWCNTs used in this study presented a low but measurable 6.0 % O 1s compositional value.⁴⁰ Thus, correlating weight data patterns of successful iron complexes to increasing concentrations of oxygenated defects in the 6.0–27.2 % range for the O 1s compositional values may be readily performed. Such a correlation graph may form an unusual basis towards a wet-chemistry based tracking of the quality level of industrially processed CNTs (Quality-Control standardization).

4. Conclusion

In summary, we have demonstrated that neutral irontricarbonyl complexes, **1a**, and **3a–8a**, enabled the reversible and quantified decoration of MWCNTs toward novel iron-complexed functional MWCNT-based nanocomposites. A rationalizing model of nonbonding interactions that developed during iron complex adsorption onto MWCNT sidewalls has been proposed leading to a better understanding of adsorption phenomena. GMMX-minimized structures of all successfully adsorbed iron complexes, as well as selected unsuccessfully adsorbed ones, well supported the validity of the proposed model. Additionally, this methodology has been tested on oxidized MWCNTs, which presented oxygenated surface defects. Obtained results emphasized the fact that fabrication and/or purification protocols of MWCNTs that generated such sidewall defects may strongly influence the efficiency of non-covalent adsorptions of η^4 -dienyl-iron complexes onto MWCNT sidewalls. Various applications of this novel methodology of MWCNT functionalization, which may be readily tracked by FT-IR spectroscopy, are in progress in our laboratory, such as the FT-IR imaging of chemically-modified single/multi-walled CNTs in diverse cell cultures for toxicity studies.

Acknowledgements

This work has been supported by the Special Internal Research Fund of Bar-Ilan University (Research Authority, Ramat-Gan, Israel).

References and notes

- 1 S. R. Wilson, *Biological aspects of fullerenes*, in *Fullerenes: Chemistry, Physics and Technology*, John Wiley and Sons, Inc., New York, 2000, ch. 10, pp. 437–466.
- 2 H. Dai, *Acc. Chem. Res.*, 2002, **35**, 1035.

- 3 P. M. Ajayan, *Chem. Rev.*, 1999, **99**, 1787.
- 4 K. Balasubramanian and M. Burghard, *Small*, 2005, **1**, 180.
- 5 A. Hirsch, *Angew. Chem., Int. Ed.*, 2002, **41**, 1853.
- 6 Y.-P. Sun, K. Fu, Y. Lin and W. Huang, *Acc. Chem. Res.*, 2002, **35**, 1096.
- 7 S. Banerjee, M. G. C. Kahn and S. S. Wong, *Chem.–Eur. J.*, 2003, **9**, 1898.
- 8 D. Tasis, N. Tagmatarchis, V. Georgakilas and M. Prato, *Chem.–Eur. J.*, 2003, **9**, 4000; R. M. Reilly, *J. Nucl. Med.*, 2007, **48**, 1039.
- 9 K. M. Lee, D. W. Chang, F. Y. Yang and D. Liming, *Polym. Prepr. (Am. Chem. Soc., Div. Polym. Chem.)*, 2005, **46**, 197; D. Hill, Y. Lin, L. Qu, A. Kitaygorodskiy, J. W. Connell, L. F. Allard and Y.-P. Sun, *Macromolecules*, 2005, **38**, 7670.
- 10 R. Zanella, E. V. Basiuk, P. Santiago, V. A. Basiuk, E. Mireles, I. Puente-Lee and J. M. Saniger, *J. Phys. Chem. B*, 2005, **109**, 16290; B. R. Azamian, K. S. Coleman, J. J. Davis, N. Hanson and M. L. H. Green, *Chem. Commun.*, 2002, 366.
- 11 V. Georgakilas, K. Kordatos, M. Prato, D. M. Guldi, M. Holzinger and A. Hirsch, *J. Am. Chem. Soc.*, 2002, **124**, 760; N. Tagmatarchis and M. Prato, *J. Mater. Chem.*, 2004, **14**, 437.
- 12 J. L. Stevens, A. Y. Huang, H. Q. Peng, L. W. Chiang, V. N. Khabashesku and J. L. Margrave, *Nano Lett.*, 2003, **3**, 331.
- 13 P. R. Marcoux, J. Schreiber, P. Batail, S. Lefrant, J. Renouard, G. Jacob, D. Albertini and J. Y. Mevellec, *Phys. Chem. Chem. Phys.*, 2002, **4**, 2278.
- 14 J. L. Bahr, J. P. Yang, D. V. Kosynkin, M. J. Bronikowski, R. E. Smalley and J. M. Tour, *J. Am. Chem. Soc.*, 2001, **123**, 6536.
- 15 X. Wang, Y. Liu, W. Qiu, D. Zhu and D., *J. Mater. Chem.*, 2002, **12**, 1636.
- 16 J. Zhao, J. P. Lu, J. Han and C.-K. Yang, *Appl. Phys. Lett.*, 2003, **82**, 3746.
- 17 G. Chambers, C. Carroll, G. F. Farrell, A. B. Dalton, M. McNamara, M. in Het Panhuis and H. J. Byrne, *Nano Lett.*, 2003, **3**, 843.
- 18 M. J. O'Connell, P. Boul, L. M. Ericson, C. Huffman, Y. Wang, E. Haroz, C. Kuper, J. Tour, K. D. Ausman and R. E. Smalley, *Chem. Phys. Lett.*, 2001, **342**, 265.
- 19 A. Star and J. F. Stoddart, *Macromolecules*, 2002, **35**, 7516; J. U. Lee, J. Huh, K. H. Kim, C. Park and W. H. Jo, *Carbon*, 2007, **45**, 1051.
- 20 V. C. Moore, M. S. Strano, E. H. Haroz, R. H. Hauge, R. E. Smalley, J. Schmidt and Y. Talmon, *Nano Lett.*, 2003, **3**, 1379.
- 21 R. J. Chen, Y. Zhang, D. Wang and H. Dai, *J. Am. Chem. Soc.*, 2001, **123**, 3838; Z. Guo, P. J. Sadler and S. C. Tsang, *Adv. Mater.*, 1998, **10**, 701; W. Zheng and Y. F. Zheng, *Electrochem. Commun.*, 2007, **9**, 1619.
- 22 M. S. Arnold, M. O. Guler, M. C. Hersam and S. I. Stupp, *Langmuir*, 2005, **21**, 4705; L. S. Witus, J.-D. R. Rocha, V. M. Yuwono, S. E. Paramonov, R. B. Weisman and J. D. Hartgerink, *J. Mater. Chem.*, 2007, **17**, 1909.
- 23 R. Grée, R. and J.-P. Lellouche, *Advances in Metal-Organic Chemistry*, 1995, **4**, 129.
- 24 W. A. Donaldson, *Aldrichimica Acta*, 1997, **30**, 17.
- 25 W. A. Donaldson, *Curr. Org. Chem.*, 2000, **4**, 837.
- 26 G. Jaouen, *Pure Appl. Chem.*, 1986, **58**, 597.
- 27 A. Vessieres, S. Tondou, G. Jaouen, S. Top, A. A. Ismail, G. Teutsch and M. Moguilewsky, *Inorg. Chem.*, 1988, **27**, 1850.
- 28 A. J. Birch and L. F. Kelly, *J. Organomet. Chem.*, 1985, **286**, C5.
- 29 M. Uemura, T. Minami, Y. Yamashita, K. Hiyoshi and Y. Hayashi, *Tetrahedron Lett.*, 1987, **28**, 641.
- 30 All the acyclic neutral η^4 -(1E,3E)- and cationic η^5 -pentadienyl-Fe(CO)₂L (L = CO or PPh₃, Scheme 1) iron complexes have been previously described. See the following references for detailed characterization data: **1a** (G. F. Docherty, G. R. Knox and P. L. Pauson, *J. Organomet. Chem.*, 1998, **568**, 287), **1b** (J. A. S. Howell, A. G. Bell, P. J. O'Leary, G. R. Stephenson, M. Hastings, P. W. Howard, D. A. Owen, A. J. Whitehead, P. McArdle and D. Cunningham, *Organometallics*, 1996, **15**, 4247), **2a** (K. Godula, H. Baermann and W. A. Donaldson, *J. Org. Chem.*, 2001, **66**, 3590), **2b** (J. A. S. Howell, A. G. Bell, D. Cunningham, P. McArdle, T. A. Albright, Z. Goldschmidt, H. E. Gottlieb and D. Hezroni-Langerman, *Organometallics*, 1993, **12**, 2541), **3a**, **4b**, **3b**, **4a**, **5a**, **6a**, **5b**, **6b** (L. Motiei, I. Marek, H. E. Gottlieb, V. Marks and J.-P. Lellouche, *Tetrahedron Lett.*, 2003, **44**, 5909), R. Schobert, H. Pfab, A. Mangold and F. Hampel, *Inorg. Chim. Acta*, 1999, **291**, 91), **8a** (J. A. S. Howell, M. G. Palin, G. Jaouen, S. Top, H. El Hafa and J. M. Cense, *Tetrahedron: Asymmetry*, 1993, **4**, 1241), **9a** (J. A. S. Howell, A. D. Squibb, A. G. Bell, P. McArdle, D. Cunningham, Z. Goldschmidt, H. E. Gottlieb, D. Hezroni-Langerman and R. Grée, *Organometallics*, 1994, **13**, 4336), **10a** (S. V. Ley, L. R. Cox, G. Meek, K.-J. Metten, C. Pique and J. M. Worrall, *J. Chem. Soc., Perkin Trans. 1*, 1997, 3299), and **11a**, **11b**, **12a**, **12b** (W. A. Donaldson, *Aldrichimica Acta*, 1997, **30**, 17).
- 31 Both Fig. 2A and C disclosed several bundles of the iron-complexed composite MWCNT-**5a**, which possess variable diameters (130 nm–1.0 μ m). This is due to a more or less pronounced level of irreversible association/aggregation of *parallel arranged* individual nanotubes. This aggregation phenomenon is likely to arise from hydrophobic and/or van der Waals interactions may be commonly observed during the TEM/SEM microscopy characterization of any functional and non-functional nanomaterial. Relating to the composite MWCNT-**5a**, measured diameters of bundles account for the aggregation of around *three to twenty five* individual nanotubes. This aggregation feature has been fully exploited for a *more sensitive* detection of the iron (Fe) element by compositional EDAX elemental analysis during HR-TEM/HR-SEM investigations (Fig. 2C, 2D, 2F and 2G). Indeed, compositional EDAX analysis is usually considered as not being a very sensitive method.
- 32 Some homogeneously distributed red/white spots that account for Fe can also be distinguished in the green/black backgrounds of the STEM mapping microphotographs. Likely resulting from the partial desorption of the iron complex **5a**, they appeared less concentrated than on the carbon materials. This phenomenon arose from two synergistic factors, *i.e.* the sample preparation that used *ultrasound* in order to correctly suspend the MWCNT-**5a** composite in EtOH before deposition on the Cu grid, and the *24 h long* high-energy electron irradiation of the sample necessary for the STEM mapping analysis. It should be noted that TGA analyses of all the iron-complexed MWCNT-based composites indicated that these complexes may be burnt/decomposed in a *low*, 117–252 °C, temperature range.
- 33 F. Nunzi, F. Mercuri, A. Sgamellotti and N. Re, *J. Phys. Chem. B*, 2002, **106**, 10622.
- 34 F. Nunzi, F. Mercuri and A. Sgamellotti, *Mol. Phys.*, 2003, **101**, 2047.
- 35 M. S. Dresselhaus, G. Dresselhaus, A. Jorio, A. G. Souza Filho and R. Saito, *Carbon*, 2002, **40**, 2043.
- 36 A. Jorio, M. A. Pimenta, A. G. Souza Filho, R. Saito, G. Dresselhaus and M. S. Dresselhaus, *New J. Phys.*, 2003, **5**, 139.
- 37 N. A. Clinton and C. P. Lillya, *J. Am. Chem. Soc.*, 1970, **92**, 3058.
- 38 J. Liu, A. G. Rinzler, H. Dai, J. H. Hafner, R. K. Bradley, P. J. Boul, A. Lu, T. Iversen, K. Shelimov, C. B. Huffman, F. Rodriguez-Macias, Y.-S. Shon, T. R. Lee, D. T. Colbert and R. E. Smalley, *Science*, 1998, **280**, 1253.
- 39 S. S. Wong, E. Joselevich, A. T. Woolley, C. L. Cheung and C. M. Lieber, *Nature*, 1998, **394**, 52.
- 40 Multi- and single-walled CNTs are usually cleaned from metal catalysts using oxidizing and/or non-oxidizing acidic treatments (see also ref. 5 and 7 for standard conditions). Therefore, unadapted non-optimized cleaning methods used during the industrial processing of CNTs likely cause the formation of detrimental surface concentrations of oxygenated defects onto CNT sidewalls. This fact may seriously compromise the optimization of a vast range of reversible/irreversible reactions operating on CNT sidewalls like the one disclosed in this study.